Curvature effect in the longitudinal unzipping carbon nanotubes

G. L. Luque, M. I. Rojas & E. P. M. Leiva

Journal of Solid State Electrochemistry
Current Research and Development in Science and Technology

ISSN 1432-8488
Volume 17
Number 4

J Solid State Electrochem (2013)
17:1189-1200
DOI 10.1007/s10008-012-1992-0

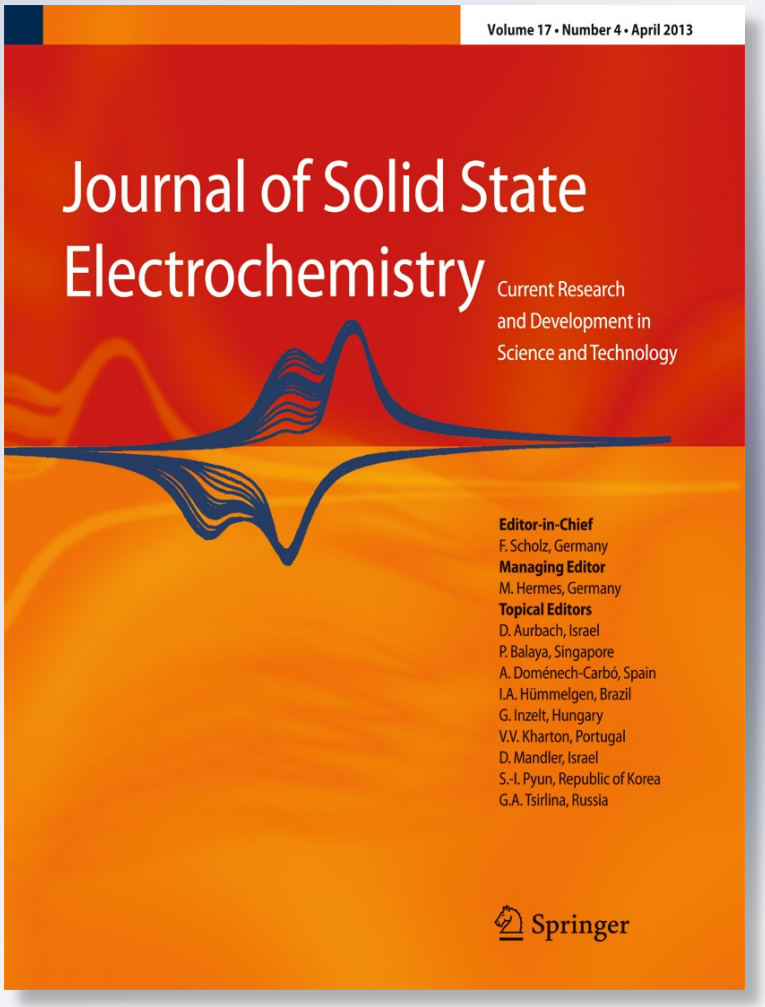

Springer

J Solid State Electrochem (2013) 17:1189–1200
DOI 10.1007/s10008-012-1992-0

ORIGINAL PAPER

Curvature effect in the longitudinal unzipping carbon nanotubes

A DFT study

G. L. Luque · M. I. Rojas · E. P. M. Leiva

Received: 29 November 2012 / Revised: 21 December 2012 / Accepted: 25 December 2012 / Published online: 8 January 2013

Abstract Density functional theory (DFT) calculations are performed to analyze curvature effects in the oxidative longitudinal unzipping of carbon nanotubes (CNTs) of different diameters. The reactions considered involve the adsorption of permanganate, followed by the oxidation of the nanotube, which results in dione and hole formation. The study was performed with armchair CNTs of different diameters and with corrugated graphene layers, which emulate the curvature of CNT of larger radii, with the finding that the curvature and the pyramidalization angle of the these structures strongly affects the stability of the intermediate dione structure formed during the unzipping process. Permanganate adsorption energies increase for more curved surfaces promoting the oxidation reaction in surfaces of small radius, making this reaction spontaneous for small radius. The second permanganate adsorbs on the parallel carbon–carbon bond to first diona formation resulting the longitudinal unzipping of the CNT.

Keywords Graphene nanoribbons · Carbon nanotube · Unzipping · Density functional theory

Introduction

Since the finding that graphene can be mechanically separated from graphite [1] to obtain 2D strips of carbonaceous material of one layer thickness, where the sp^2 bonded carbon atoms are arranged in a honeycomb lattice, theoretical and experimental groups have researched this material intensively. This is due to its unique electronic, mechanical, optical, magnetic and biocompatible properties, which makes it a promising material for several technological applications in electronics, biosensor manufacturing [2–4], or for hydrogen storage [5–8], among others [9, 10]. This type of materials receives considerable interest is the field of electrochemistry [11], where graphene has been reported to be beneficial in various applications ranging from sensing through energy storage and generation and carbon based molecular electronics [3].

The extension of graphene in one direction yields graphene nanoribbons (GNRs) of rectangular shape, zig-zag or armchair straight edges with a given width. These geometric arrangements can be obtained from graphite oxide by means of chemical or synthetic procedures [12–15]. Depending on the width of the GNRs, their electrical properties change from semimetallic to metallic ones, putting into evidence the importance that edges have in the electrical properties of the GNRs [16–18]. Nevertheless, it is difficult to obtain a complete set of smooth edges and controllable widths. Recently, Kosynkin et al. [19] and Higginbotham et al. [20] were able to obtain GNRs of zigzag edges, opening longitudinally multi-wall carbon nanotubes (CNTs) by a chemical treatment with a solution of potassium permanganate in acid medium. The widths of graphene ribbons that can be obtained unzipping armchair (*n*,*n*) CNT are listed in Table 1.

The opening mechanism proposed was inspired in the oxidation of alkenes by permanganate. These authors suggested the formation of an ester of manganese on an unsaturated bond of the nanotube side wall as the first and rate-determining step, followed by oxidation of the carbons to produce a dione and producing a hole on the CNT. An important feature of this procedure is that GNRs can be obtained in a significant number, which is an important factor for their application in different electrochemical

G. L. Luque · M. I. Rojas (✉) · E. P. M. Leiva
INFIQC, Departamento de Matemática y Física,
Facultad de Ciencias Químicas, Universidad Nacional de Córdoba,
Ciudad Universitaria, 5000 Córdoba, Argentina
e-mail: mrojas@fcq.unc.edu.ar

Table 1 Radius of different CNT and the corresponding width of the related nanoribbons

System	r[Å]	$2\pi r$[Å]
(4,4)	2.71	17.03
(6,6)	4.06	25.51
(8,8)	5.42	34.05
(10,10)	6.77	42.54
(12,12)	8.13	51.08

devices. In this way Kosynkin et al. [19] and Higginbotham et al. [20] obtained oxidized graphene nanoribbons (oxGNRs) that have the unique ability to form stable aqueous dispersions and have high bio-compatibility, and possess good electrocatalytic properties [21]. Even more, the reduction of this material produces graphene with potential applications in diverse fields [2–10]. Recent studies [22] have demonstrated the electrochemical Li intake capacity of GNRs obtained by unzipping multiwall CNTs, making these systems also attractive for energy storage in Li-ion battery devices.

Recently, quantum mechanical calculations [23, 24] were performed to study the opening mechanism of armchair CNTs. It was suggested that the opening begins with the breaking of a C–C bond placed in the wall and goes on in the longitudinal direction of the nanotube axis. Since some of these results suggested that the size of the nanotubes may play a role in this phenomenon, we decided to develop a model that allows the first-principles systematic study of curvature effects in nanotubes of arbitrary radius, with a modest computational effort. With this tool, we present in this work a study of the unzipping mechanism and the kinetics of CNTs opening to give GNRs of zigzag edges, as a function of curvature radius. We consider a set of armchair CNTs of different radii, as well as corrugated graphene sheets (CGS) which emulate the curvature of CNT of larger radii [25]. This approach was found useful to reduce the number of atoms and so the computational cost. Thus, we could study a wide range of nanotube radii involving only 80 carbon atoms in the calculations.

Model and computations

Density functional theory (DFT) calculations were performed employing the SIESTA computer code [26, 27]. A localized basis set composed of double $-\zeta$ plus polarization was used. The basic functions were numerical atomic orbitals (NAOs), the solutions of the Kohn-Sham Hamiltonian for the isolated pseudoatoms. Exchange and correlation effects were described using a generalized gradient approximation (GGA), within the Perdew–Burke–Ernzerhof (PBE) functional [28]. The core electrons were replaced by norm conserving pseudopotentials [29] in their fully separable form [30]. In the pseudopotential description of the atoms, only valence electronic states were considered. The value of the confinement parameters were defined variationally applying the simplex method [31]. The cut-off of the grid for real-space integrals [26] yielded converged results for all the systems studied here using a value of 150 Ry. All the

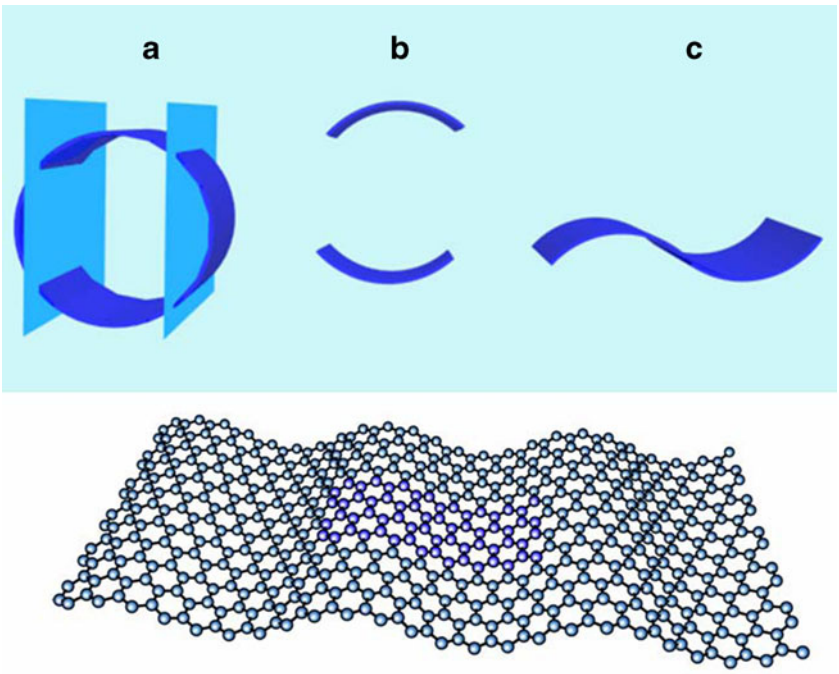

Fig. 1 Scheme devised to represent carbon atoms in nanotubes of different widths using corrugated sheets. The aim is to have carbon atoms whose close environment is chemically similar to that of nanotubes with the same curvature radius. *Top*: **a** the entire nanotube and the position of the planes used to select atoms; **b**the atoms belonging to the two curved surfaces; **c** the corrugated surface formed by joining the two surfaces. *Bottom*: corrugated sheet with atoms of the unit cell highlighted in *blue*

calculations were performed with spin polarization (sp). Since the SIESTA code uses periodic supercells to represent the system, each of these units must be neutral to keep the energy of the system finite. For this reason, in the case of the permanganate adsorption, the reference system was an isolated, neutral (radical) MnO_4. The binding energy of the permanganate ion could be recovered by considering the electron affinity of MnO_4 and the work function of the carbonaceous nanostructure. Upon adsorption, Mulliken analysis showed that the MnO_4 unit properly acquired a negative charge, as expected. Comparative calculations with an extra negative charge on the electronic system, compensated by a homogeneous positive background yielded geometries for the adsorbed permanganate species that were indistinguishable from those obtained with neutral slabs.

The minimum energy configuration was obtained with the conjugate gradient (CG) technique [31], minimizing the energy of the system from an initial configuration with respect to the atomic coordinates. The charges on the different atoms were evaluated by means of the Mulliken population analysis [32].

We perform calculation with a set of armchair CNTs which have a curvature radius in the interval [2.7 Å; 8.1 Å]. The CNT studied comprised the set (4,4); (5,5); (6,6); (8,8); (10,10); (12,12), which involve unit supercells with 80, 100, 120, 160, 200, 240 atoms, respectively; with periodic boundary conditions in *x*, *y*, *z* representing the CNTs of infinite length.

In order to deal with the problem of calculating systems with a larger number of atoms in the supercell, we developed an approach to represent the CNTs by means of corrugated sheets (named by CGS in figures), where carbon atoms in the sheet have a close environment that emulates that present in the CNTs. Thus, CGSs were designed using 80-carbon-atom basis for all radii, where the carbon atoms are arranged in a honeycomb pattern, as shown in Fig. 1.

The unit cell was tetragonal with periodic boundary conditions in *x*, *y*, *z* directions imposed in order to represent an infinite surface. The position of the vertical two planes determines the length of the arc, which must be equal to half of the length of the GNR of 80 atoms. In the case of (4,4) CNT, we do not obtain any reduction in number of atoms because the two halves are complete, only splitted to give the corrugated sheet. However, this system provides a benchmark to test the present approximation.

Results and discussion

In order to analyze the correlation between results obtained with the model of CGSs and those obtained with CNTs, we evaluated the nanostructure formation energy, which gives

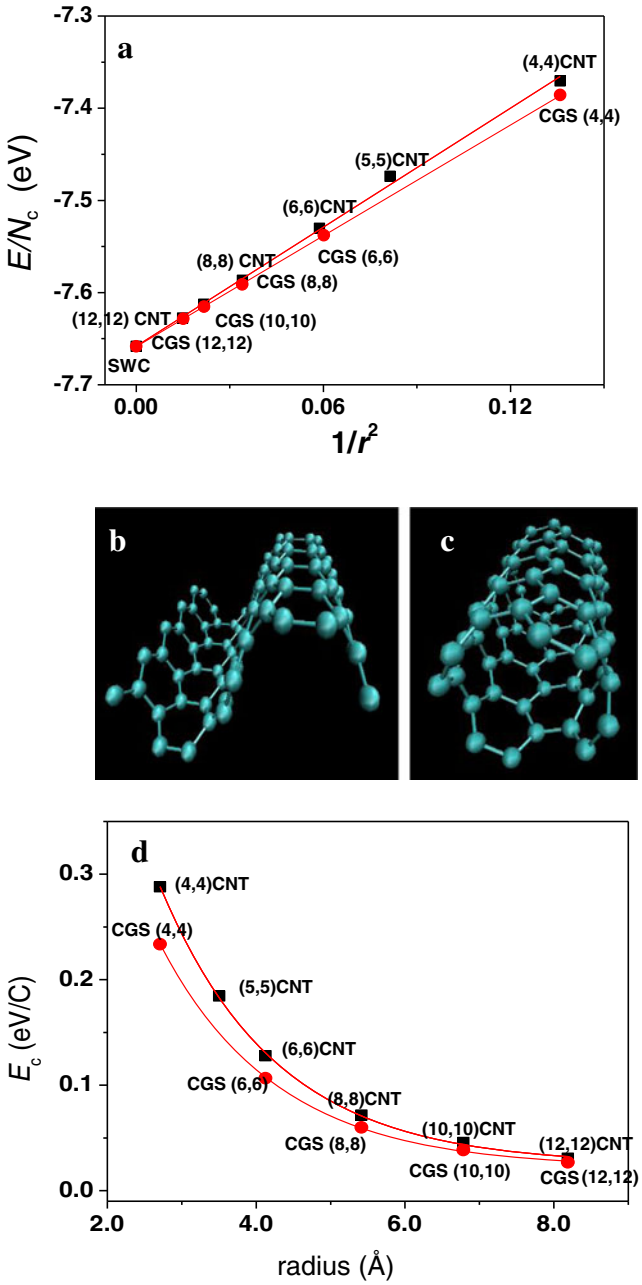

Fig. 2 **a** Formation energy of different carbon nanostructures as function of the reciprocal of the square of the curvature radius. **b**, **c** A (4,4) corrugated sheet and a (4,4) nanotube, respectively. **d** Curvature energy per carbon atom, E_c, as a function of curvature radius

Table 2 Parameters of the least-squares fitting of the results corresponding to the CNTs systems and corrugated surfaces presented in Fig. 2a

Parameters	CNT	Corrugated graphene
Slope [eV Å]	−2.15	−2.00
Intercept [eV]	−7.66	−7.66

Table 3 Hybridization of σ-orbitals (sp^n), p content of the σ-orbital ($n=3m+2$)

	(4,4)	(5,5)	(6,6)	(8,8)	(10,10)	(12,12)	SWC
Radio (Å)	2.71	3.50	4.07	5.42	6.78	8.19	∞
n of C of CGS	2.1		2.05	2.04	2.02	2.01	2.0
n of C of CNT	2.1	2.07	2.04	2.03	2.02	2.01	
n of C of CGS-MnO_4	3		2.6	2.48	2.44	2.43	2.43
n of C of CNT-MnO_4	3	2.37	2.49	2.45	2.45		

information about the stabilization of an atom in a given lattice with respect to the isolated carbon in vacuum. The formation energy was calculated according to:

$$E_{\text{formation}} = \frac{E_{\text{total}}}{N} - E_{\text{C}}^{\text{vacuum}} \quad (1)$$

where E_{total}/N is energy per atom in the lattice, and $E_{\text{C}}^{\text{vacuum}}$ is the energy of a non-interacting carbon atom in vacuum. Figure 2a shows the formation energies calculated for the CNTs (black) and corrugated graphene (red) as function of the reciprocal of the square of the curvature radius *r*. It is interesting to compare the result obtained for the (4,4) corrugated sheet (Fig. 2b) with that of the (4,4) CNT (Fig. 2c), since for these systems the largest deviation is expected.

It is found that systems with the same index present an excellent correlation (see Table 2), decreasing the differences with the increase in the index number (greater systems).

It must be emphasized that the comparison of formation energies (Eq. 1) between corrugated surfaces and nanotubes is a very stringent test to the model, for the present calculation aims. In fact, we are pursuing the calculations of reaction energies, which are rather sensitive to the local chemical properties than to the whole geometry of the system. Thus, we employed the corrugated slab approach to represent the whole set of CNTs without a considerable increase of computational cost, since the proposed model simulates different CNTs with only 80 carbon atoms, independent of their radii.

All the calculations employing corrugated sheets were performed fixing the size of the simulation cell, because cell relaxation would deliver a planar structure, which is that of minimum energy, as it can be seen in the intercept (0, −7.7 eV) of the straight line with the vertical axis in Fig. 2a, at $1/r^2 \to 0$.

In order to consider the effect of curvature on the energetics of the different carbonaceous surfaces, we define a curvature energy (E_c) as: $E_c = E_{\text{formation}}(\text{CNT(n,n)}) - E_{\text{formation}}(\text{SWC})$, where $E_{\text{formation}}(\text{SWC})$ is the formation energy of the graphene layer. E_c is shown in Fig. 2d as a function of the curvature radius, where it is found that this quantity amounts up to 0.3 eV for the thinnest nanostructures. As expected from Fig. 2a, E_c is proportional to $1/r^2$, as shown by Robertson et al. [33] and Tibbets [34] using classical elasticity arguments

$$E_c = \frac{Yd^3}{24}\frac{\Omega}{r^2} = \frac{\alpha}{r^2} \quad (2)$$

where *Y* is Young's modulus, *d* is the interplanar space in graphite and Ω is the surface occupied by a carbon atom. The value of α in Eq. 2 may be fitted by least squares obtaining $\alpha_{\text{CNTs}} = 2.14$ eV A^2/atom in the case of CNTs, in good agreement with the literature [35, 36]. In the case of the corrugated layers, we obtain $\alpha_{\text{corrugated}} = 1.72$ eV A^2/atomÅ.

In general, the chemical reactivity of a CNT is mainly driven by the strain of the local atomic structure, reflected in the pyramidalization angles [37, 38] of the carbon atoms, which is a gauge of the local curvature. In CNT or CGS, the p orbitals are not parallel to each other and C atoms are not sp^2 hybridized as those in graphite. As the diameter of CNT increases, the hybridization will be close to sp^2, the curvature induces pyramidalization and misalignment of π-orbitals (being the main source of strain in CNTs) producing a local strain, delivering more reactive structures than a flat graphene sheet. In order to analyze how strain force and hybridization of C atoms change with increasing diameter of CNT, we performed π orbital axis vector (POAV) analysis with the program developed by Haddon [39]. The

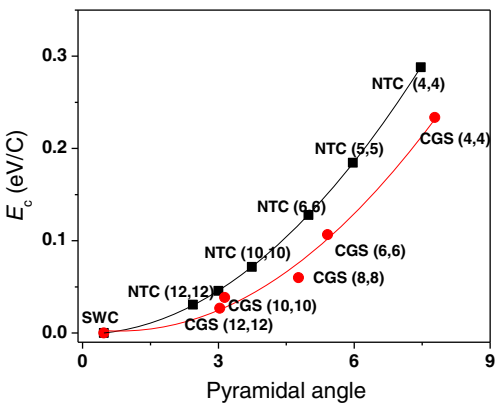

Fig. 3 Curvature energy, E_c, per carbon atom versus pyramidal angle for CNTs (*black filled square*) and corrugated surfaces (*red filled circle*)

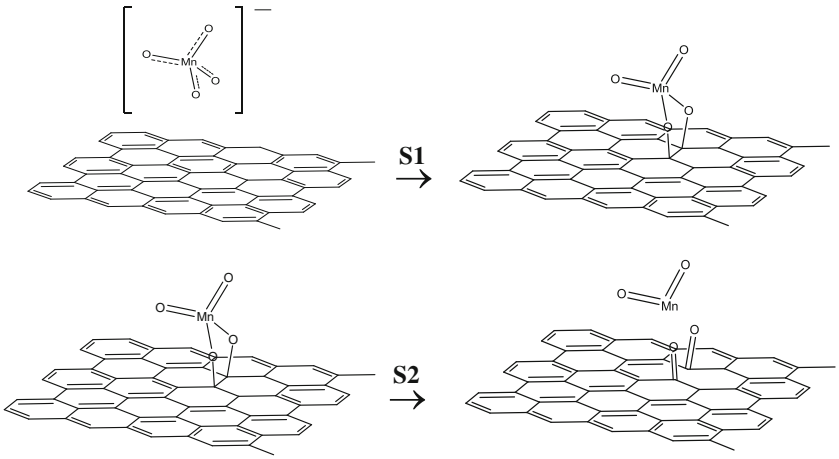

Fig. 4 Steps proposed for the initiation of the unzipping of a carbon nanotube, illustrated for a portion of a graphenic surface. *S1*: the reaction starts with the adsorption of permanganate forming an ester. *S2*: oxidation takes place yielding a dione and a hole on the surface

pyramidalization angle for planar sp^2 is 0° and 19.74° for a tetrahedral sp^3 hybridized carbon [40].

The hybridization is expressed as the p content of σ-orbitals (sp^n) and the s content of the π-orbitals (s^mp) [41, 42]. Haddon [37] and Niyogi et al. [37, 38] have reported that pyramidalization and π-orbital misalignment angles decrease as the radio increases, which is here evident from the data presented in Table 3 and Fig. 3. The curvature energy increases with pyramidalization and π-orbital misalignment angles indicating that there is more strain in smaller diameter CNT or corrugated graphene. It is the relief of this strain that drives the chemistry of CNTs as stability increases with the increment of the diameter [43]. As the CNT or corrugated graphene layer radio increases, the sp^2 character of the carbons increases as can be seen in Table 3.

Curvature effect of the CNT oxidation reaction

Unzipping of CNTs by the chemical method proposed by Kosynkin et al. [19] and Higginbotham et al. [20] is produced by an oxidation reaction (ORCNT), achieved using a solution of potassium permanganate in acidic medium, yielding MnO_2 and the ORCNT according to:

$$MnO_4^- + CNT \rightarrow CNTO_2 + MnO_2 \quad (3)$$

Figure 4 shows the most simple two-step scheme that can be proposed for the ORCNT, illustrated for a portion of a graphenic surface. The first step consists in the formation of a manganate ester (Fig. 4, S1). The following step, S2, shown in Fig. 4, is the reaction of the adsorbed permanganate to yield a diona adsorbed species.

The first step is claimed to be the rate-determining step in the opening mechanism [19], while the second is assumed to be fast. We will show that this may be true for strongly curved surfaces, but will also demonstrate that the second step may slow down the reaction and even become energetically unfavourable for CNT with large curvature radius.

According to the previous scheme, we started with the final state of step S1, that is, the consideration of the structures of permanganate bonded to corrugated graphene and CNTs of different diameters by means of CG minimizations of the total energy.

Figure 5 shows the initial (left) and optimized geometries (right) of permanganate bonded to a graphene layer (infinite curvature radius) and to a (5,5) CNT (3.5 Å of radius). While in the first case (Fig. 5b) the binding of the permanganate ester does not produce the formation of the diona, in the case of the (5,5) CNT (Fig. 5d) the oxidation of the surface is produced along with diona formation and the subsequent opening without any energy barrier.

This is a common feature for all nanostructures with curvature radii smaller than 3.5 Å. For the smaller nanotubes, dione formation upon minimization was obtained

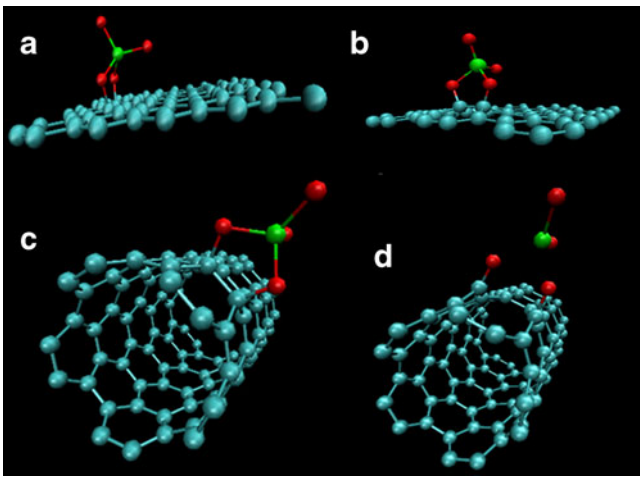

Fig. 5 Initial and final states for the formation of a dione on different graphenic systems starting from adsorbed permanganate. Initial (**a**) and final (**b**) states for permanganate adsorption on a graphene layer; initial (**c**) and final (**d**) states for permanganate adsorption on a (5,5) CNT

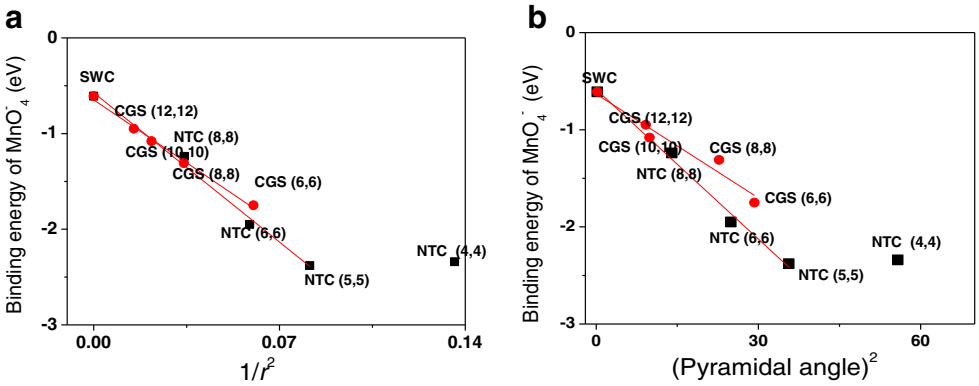

Fig. 6 Binding energy of permanganate upon adsorption on different CNTs (*black filled square*) and corrugated surfaces (*red filled circle*) as a function of the reciprocal of the square of the curvature radius (**a**). As a function of the square of pyramidalization angle (**b**)

choosing an initial configuration where the oxygen atoms are located at 1.45 Å from the closest C atoms and these O to 1.81 Å form manganese atom, in the carbonaceous nanostructure. When the permanganate molecule was located farther away from the closest C atoms than 1.48 Å, we found a local minimum, without the spontaneous formation of the dione, in agreement with literature results [23, 24].

It is illustrative to relate spontaneous dione formation to previous knowledge gained on the effect that curvature produces on the bonds and the energetics of the carbon nanostructure. Sánchez-Portal et al. studied [36] the structural and elastic properties of CNTs of different radii and chiralities, with two remarkable findings: first, an increase in C–C bond lengths (as compared with graphene) with decreasing curvature radius; second, an increase in the difference between both types of C–C bonds, where the longer bonds are those perpendicular to the tube axis. These results indicate a rehybridization and weakening of the π bonds induced by curvature as was previously discuss in the changes observed in the pyramidalization angles whit curvature, which is consistent with the increased reactivity that we observed in the nanotubes with curvature radius smaller than 3.5 Å. From an energetic viewpoint, this situation correspond to curvature energies larger than 0.11 eV/atom. Figure 5a and b shows how two C atoms of the graphene layer change their hybridization from sp^2 to sp^3 upon manganate ester formation. Concomitantly, the C–C distance of the bond involved increases from 1.42 to 1.58 Å and the C–C–C angles change from 120° to 110°. On the other hand, Fig. 5c and d show that in the case of (5,5) CNT the C–C distance increases from 1.43 to 2.72 Å due to the formation of the diona.

Since the radius of the CNT or graphene layer plays a very important role in the energetics of the system, we studied the adsorption energies of permanganate on CNTs and corrugated graphene of different curvature radii, with the results presented in Fig. 6. It can be observed there that the binding energy becomes larger in absolute value for the more curved surfaces, presenting a linear relationship with the reciprocal of the square of the curvature radius of the graphenic surface and the square of pyramidalization angle.

In Fig. 6, we also present results for the (4,4) and (5,5) CNTs, where the resulting structure upon permanganate adsorption is not the ester but the diona. As pointed out above, when the curvature radius of the CNT is smaller than 3.5 Å ((5,5) CNT) spontaneous opening with the consequent diona formation occurs. This is due to the fact that these structures present more strain energy in agreement with the results of Sun et al. [42], showing that the instability of CNT or corrugated graphene layer of smaller diameter is specially due to the non-planar distortions. This is quantitatively determined by POAV analysis (Fig. 6b). Even more, once the surface reacts with MnO_4, the carbon atom increases the sp^3 character, being this more important for surfaces of smaller diameter that relieve strain upon reaction with permanganate, as can be seen in Table 3.

The remarkable effect found for the adsorption energy of permanganate as a function of the curvature radius of the carbon nanostructure led us to a systematic study for the energy change of the system in the second step, S2, shown in Fig. 4. Figure 7 shows the energy change for S2 in Fig. 4 as a function of the curvature radius of different CNTs,

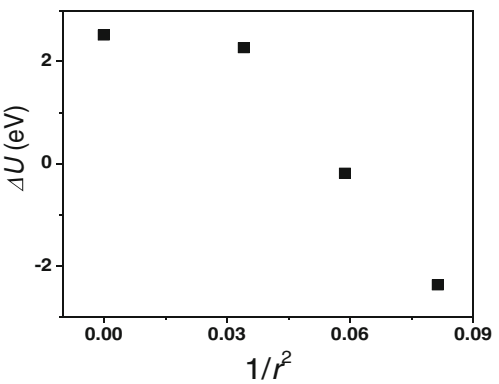

Fig. 7 Energy change ΔU corresponding to the oxidative step S2 of the unzipping reaction for nanotubes of different radius

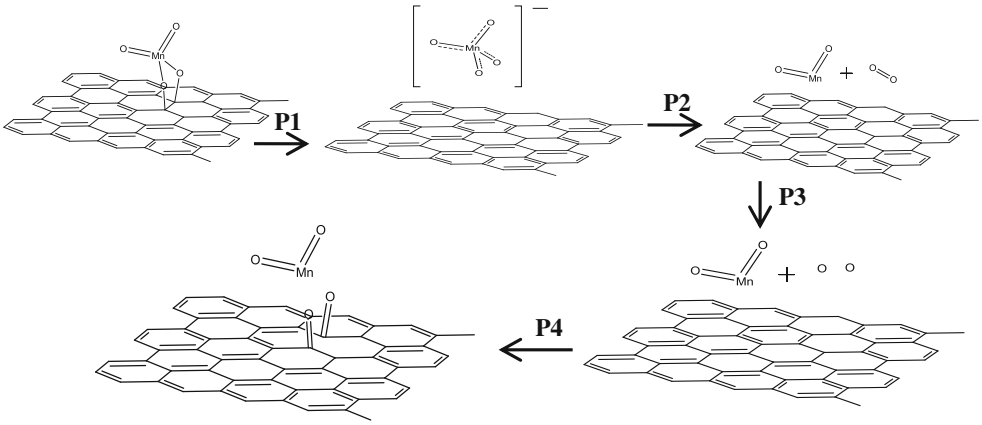

Fig. 8 Decomposition of the step S2 presented in Fig. 4 into four steps: *P1*, desorption of permanganante; *P2*, dissociation of permanganate into MnO_2 and O_2; *P3*, dissociation of O_2 in vacuum into two O atoms; *P4*, adsorption of the O atoms onto the graphenic surface to yield the diona species

where it is found that this step becomes only energetically favorable for radii smaller than 3.5 Å.

In the case of $1/r^2 = 0$ that corresponds to graphene, the ORCNT appears as the most thermodynamically unfavorable case involving an energy change of 2.57 eV. It is clear that the only physical parameter that changes the thermodynamics of S2 is the curvature of the surface. The initial and final states modify their energies with the curvature, turning the reaction from unfavourable to favourable for decreasing curvature radius. In order to understand these changes we analyzed the different energetic contributions to S2 in terms of the thermodynamic cycle shown in Fig. 8.

There, we decomposed the reaction corresponding to diona formation into four steps: P1 Desorption of permanganate, involving the permanganate desorption energy $E^{\mathrm{des}}_{\mathrm{MnO_4^-}}$; P2 Dissociation of permanganate into MnO_2 and O_2; P3 Dissociation of O_2 in vacuum into two O atoms; P4 Adsorption of the O atoms onto the graphenic surface to yield the diona species, involving the oxygen adsorption energy $E^{\mathrm{ads}}_{\mathrm{O}}$. Columns 1 and 2 in Tables 4 and 5 show the energy contributions of steps P1 and P4 for corrugated graphene and CNTs, respectively, which are the ones where the curvature of the surface plays a role.

We also show there in columns 3 and 4 the energies involved in steps P1 and P4 referred to the corresponding energy values for the plane graphene surface. From these values, we find that the energy changes involved in step P4 are more dependent on the curvature of the nanostructure than those of step P1, increasing their absolute value considerably for the most curved ones. The larger C–C distances observed between the carbon atoms involved in the formation diona (column 6) with respect to those of the carbon atoms bonded to permanganate (column 5) is consistent with the formation of a stronger C–O bond in the case of the former, as the energy data point out. This strengthening in the C–O bond is concomitant with an increase on the dione oxygen charge (column 7).

Density of states (DOS) analysis

In order to see how curvature changes reactivity on the basis of the results obtained for the different curved structures, the Partial Density of States (PDOS) was analyzed as a function of electronic energy [eV] referred to the Fermi level, for the (4,4), (6,6) and (8,8) geometries. The curvatures were assumed to be given in the *y*–*z* direction. As shown in the

Table 4 Some system properties associated with the cycle given in Fig. 8 for corrugated graphene layers

Corrugated graphene	$P1E^{\mathrm{des}}_{\mathrm{MnO_4^-}}$ [eV]	$P4E^{\mathrm{ads}}_{\mathrm{O}}$ [eV]	$\Delta E^{\mathrm{des}}_{\mathrm{MnO_4^-}}$ [eV]	$\Delta E^{\mathrm{ads}}_{\mathrm{O}}$	$d^{\mathrm{MnO_4^-}}_{\mathrm{C-C}}$ [Å]	$d^{\mathrm{dione}}_{\mathrm{C-C}}$ [Å]	$Q^{\mathrm{dione}}_{\mathrm{O}}$ [a.u.]
(6,6)	1.75	−4.88	1.14	−1.76	1.64	2.68	−0.19
(8,8)	1.31	−4.14	0.70	−1.02	1.60	2.65	−0.18
(10,10)	1.08	−3.46	0.47	−0.60	1.59	2.62	−0.17
(12,12)	0.95	−3.12	0.34	−0.34	1.59	2.61	−0.10
SWC	0.61	−3.12	0	0	1.58	2.53	−0.15

$E^{\mathrm{ads}}_{\mathrm{MnO_4^-}}$ is the desorption energy of permanganate in step P1, $E^{\mathrm{ads}}_{\mathrm{O}}$ [eV] is the energy formation of the diona starting from oxygen atoms in vacuum, step P4, $\Delta E^{\mathrm{des}}_{\mathrm{MnO_4^-}} = E^{\mathrm{des}}_{\mathrm{MnO_4^-}} - E^{\mathrm{des,SWC}}_{\mathrm{MnO_4^-}}$ and $\Delta E^{\mathrm{ads}}_{\mathrm{O}} = E^{\mathrm{ads}}_{\mathrm{O}} - E^{\mathrm{ads,SWC}}_{\mathrm{O}}$ are relative energy changes referred to the graphene monolayer, Q_{O} is the charge on the oxygen atom in the dione, $d^{\mathrm{MnO_4^-}}_{\mathrm{C-C}}$ and $d^{\mathrm{dione}}_{\mathrm{C-C}}$ are C–C distances corresponding to atoms bonded to permanganate and the dione, respectively

Table 5 Some system properties associated with the cycle given in Fig. 8 for carbon nanotubes

CNT	P1$E^{ads}_{MnO_4^-}$ [eV]	P4E^{ads}_{O} [eV]	$\Delta E^{des}_{MnO_4^-}$ [eV]	ΔE^{ads}_{O}	$d^{MnO_4^-}_{C-C}$ [Å]	d^{dione}_{C-C} [Å]	Q^{dione}_{O} [a.u.]
(6,6)	1.95	−5.52	1.34	−2.40	1.63	2.72	−0.32
(8,8)	1.24	−4.30	0.63	−1.18	1.62	2.69	−0.18
SWC	0.61	−3.12	0	0	1.58	2.53	−0.15

$E^{ads}_{MnO_4^-}$ is the desorption energy of permanganate in step P1, E^{ads}_{O} [eV] is the energy formation of the diona starting from oxygen atoms in vacuum, step P4, $\Delta E^{des}_{MnO_4^-} = E^{des}_{MnO_4^-} - E^{des,SWC}_{MnO_4^-}$ and $\Delta E^{ads}_{O} = E^{ads}_{O} - E^{ads,SWC}_{O}$ are relative energy changes referred to the graphene monolayer, Q_O is the charge on the oxygen atom in the dione, $d^{MnO_4^-}_{C-C}$ and d^{dione}_{C-C} are C–C distances corresponding to atoms bonded to permanganate and the dione, respectively

previous sections, the ORCNT is thermodynamically unfavourable for flat surfaces but it becomes spontaneous for the most curved ones. Here, we analyze how the curvature modifies the DOS which are directly related with the reactivity of the structure.

Figure 9 shows the PDOS for a C atom in the different curved surfaces. The contribution to the DOS by the 2s empty levels next to the Fermi level is found to increase with the curvature, as can be observed in Fig. 9a. The contribution of the $2p_x$ levels is roughly the same in all cases (see Fig. 9b). On the other hand, the curvature changes the contribution by $2p_y$ and $2p_z$ empty and filled levels (Fig. 9c–d). While the $2p_z$ PDOS contribution is found to increase with curvature in Fig. 9d, the $2p_y$ one is found to decrease (Fig. 9c). These trends suggest that the progressive changes found with the curvature are mainly due to the contribution of 2s and $2p_z$ orbitals.

It is worth discussing on the relevance of the previously shown DOS for an electrochemical reaction. In the case of an oxidation reaction, involving electron transfer for example from an analyte to the surface, the latter would receive electrons via the 2s, $2p_y$ and $2p_z$ levels. Thus, more curved surfaces should present a larger electroactivity. A similar consideration can be made for a reduction reaction, occurring via $2p_y$ and $2p_z$ filled levels which would supply the electrons. The curvature also modifies the electric properties of the surface via a decrease of the band gap found in the DOS graph in Fig. 9f, improving the conductive properties of the surface for smaller diameters.

Going back to the ORCNT, its first step occurs with the C–C rupture and C=O formation. After this oxidation reaction, two carbon atoms are functionalized with oxygen, which is very electronegative. This originates a charge on the surface, arising a net total spin momentum. In the case of (4,4) and (8,8) surfaces the total spin momentum are equal to $-3.23\,\mu_B$ and $-2.38\,\mu_B$, respectively. The charges on the oxygen atom increase with the curvature, as can be observed in Tables 4 and 5. Charge population analysis shows that the negative charge on the oxygen atom is not counterbalanced by a positive charge on the neighboring C atom, but rather spread on the nanotube.

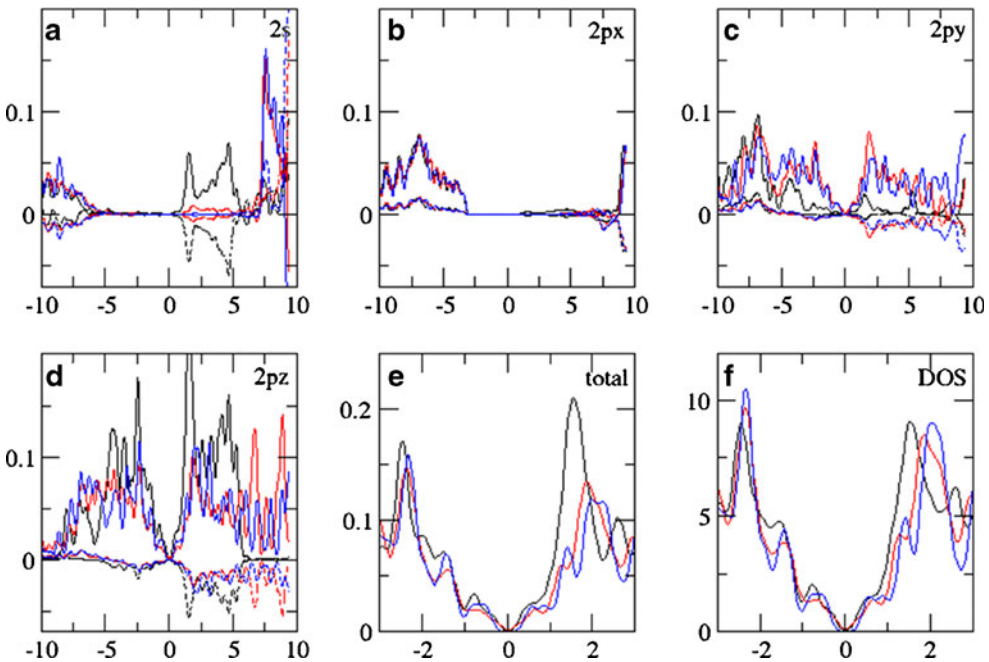

Fig. 9 Partial density of states versus energy referred to the Fermi level for a C atom on surfaces of different curvatures. *Black line* (4,4); *red line* (6,6); *blue line* (8,8) structures

Figure 10a–f and g–l shows the changes in the PDOS for the functionalized C atom in (4,4) and (8,8) structures before and after the oxidation of the surface. The greater changes are observed on the 2s, $2p_y$ and $2p_z$ orbitals which participate in the σ–π hybridization and in the formation of the new C=O bond.

The formation of the C–O bond, in the *z* direction, leads to the rupture of the C–C bond between neighboring atoms in the surface, giving place to a hole defect. All these changes are evident in the $2p_y$ and $2p_z$ PDOS (Fig. 10c–d and i–j). The surface transfers charge to the adsorbed O atom since it is more electronegative, and the magnitude of this effect depends on the curvature of the surface. While the (4,4) structure presents a huge decrease in the $2p_z$ density (Fig. 10d), the (8,8) surface has the opposite behaviour with an small increase in the PDOS (Fig. 10j).

Tables 4 and 5 show that the adsorption energy of oxygen increases (in absolute value) with the curvature. The new bond perturbs the DOS. The sum of the DOS (Fig. 10e) shows for the (4,4) structure a significantly reduction due to this carbon is charged positively while for the (8,8) one the carbon atoms is not charged and the density only changes

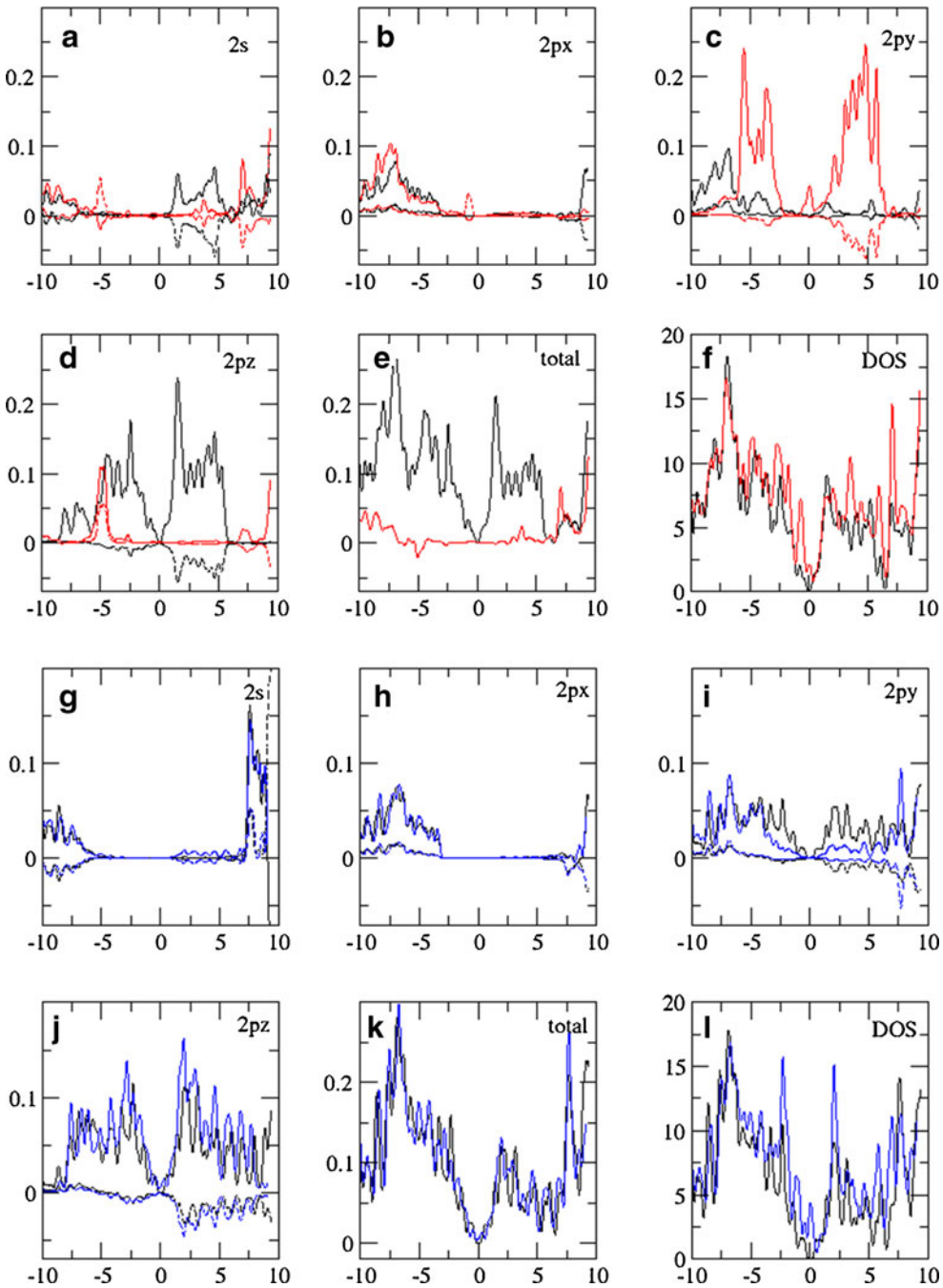

Fig. 10 The effect of the oxidation on the functionalized carbon atom. **a**–**f** For (4,4) surface: (*black line*) before and (*red line*) after the oxidation reaction. **g**–**l** For the (8,8) surface (*black line*) before and (*blue line*) after oxidation reaction

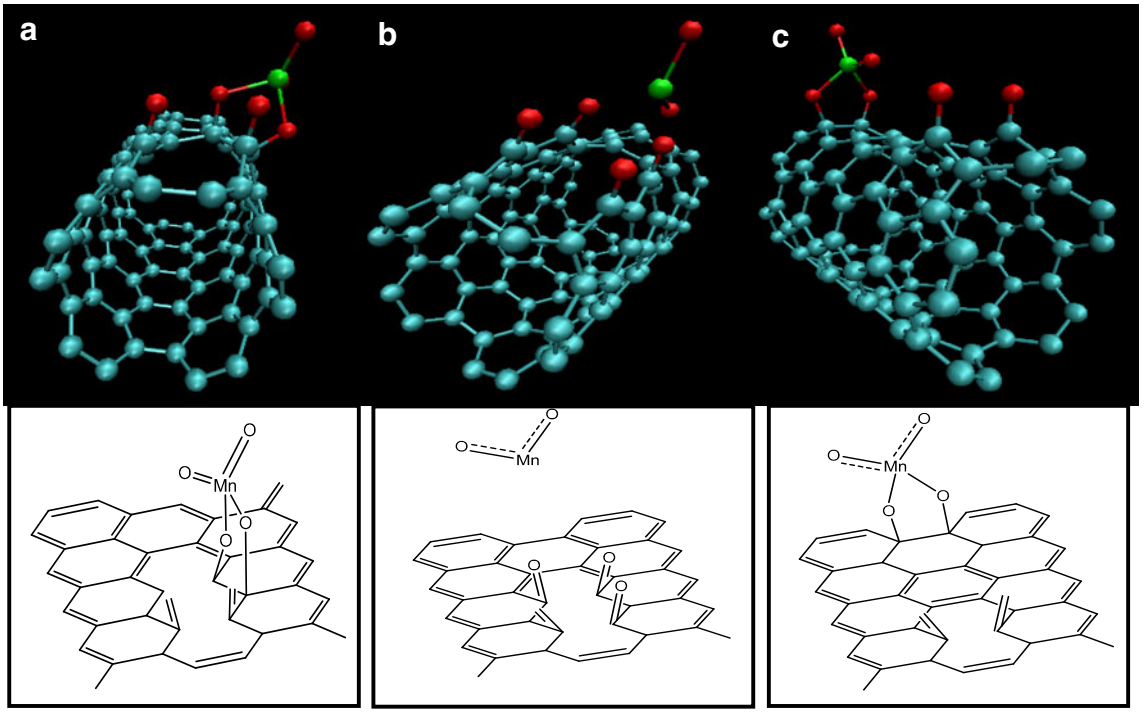

Fig. 11 Optimized geometries obtained for different binding sites of the second permanganate group

slightly (Fig. 10k). The DOS shows smaller changes in the case of (8,8) than in the case of (4,4) because in the case of (8,8) the interaction between permanganate and the graphene surface is weaker.

Longitudinal preference for nanotube unzipping

Once the first C–C rupture has occurred, the second MnO_4^- can bind to different sites. To study which of these have an increasing probability, we bind the second MnO_4^- at different sites of the (5,5) CNT. Figure 11 shows the optimized geometries obtained for different binding sites of the second permanganate group and their respective schemes. When the second MnO_4^- is bound to a neighboring but non-parallel C–C bond (Fig. 11a), the adsorption energy is smaller (−2.64 eV) than that of an adjacent parallel C–C case (−4.12 eV) (Fig. 11b).

The subsequent oxidation is facilitated, as stated before, by the repulsion produced between the two opposite carbonyl groups that produce additional strain to the adjacent C–C bond stretching it from 1.42 to 1.49 Å and making it weaker and prone to attack by permanganate. This effect is more important with increasing curvature as can be seen in column 7 of Table 5, since the charges on the O of the ketone groups are greater on more curved surfaces. The cleavage of the next C–C bond takes place to relieve strain until the CNT is fully opened to give the GNRs. The hole produced by the first rupture induce more strain and makes the adjacent bond more reactive leading to a greater binding energy, −4.12 eV and producing the rupture of this second C–C bond (it is important to notice that this energy is even larger than the binding energy of the first permanganate group, −2.38 eV, (see Table 6).

In the case of the neighboring but non-parallel C–C bond, this bond stretches from 1.42 to 1.45 Å due to the first rupture, but the next breakage does not take place. In either of these two cases the bonding energy is greater than the case where MnO_4^- is bound far from the first one (−1.78 eV) (Fig. 11c), due to the strain produced by the first rupture. This results demonstrates that the opening of the arm chair CNT occurs in a linear longitudinal cut (as shown in Fig. 11b) and not

Table 6 Binding energies for the bonded SWC and (5,5) CNT to MnO_4^- and the subsequent binding sites

	First MnO_4^- bound to SWC	First MnO_4^- bound to CNT (5,5)	Second MnO_4^- bounded to an adjacent C–C CNT (5,5)	Second MnO_4^- bounded to not an adjacent C–C CNT (5,5)
Binding energy of MnO_4^- [eV]	−0.61	−2.38	−4.12	−2.64

spiralwise (Fig. 11a) and that once the opening has begun, the total opening yields GNRs of zig-zag edges in agreement with Zhang et al. [23] and the experimental results [19].

Conclusions

The present DFT calculations where devoted to study the role of curvature on the chemical unzipping of CNTs. From the present studies, the following conclusions may be drawn:

- Initial conditions for geometry optimization can be found that lead to spontaneous ester formation or dione formation on all the carbon nanostructures considered.
- The curvature energy increases for smaller radii and greater pyramidal angle values. The effect of curvature is also evidenced in the sp^2 character hybridization that increases with the radio or pyramidal angle of the CNT or corrugated graphene surface.
- Permanganate binding energies follow a linear relationship with $1/r^2$, where r is the curvature radius of the nanostructure.
- The binding energy of permanganate follows a linear relationship with the square of the pyramidalization angle due to the relief of strain experienced by more curved surfaces upon reaction.
- Permanganate adsorption energies increase in absolute value with the bent of the surface, favouring the oxidative reaction for CNTs of small radius. The ORCNT becomes spontaneous yielding diona formation for $r \leq$ 3.5 Å, producing a hole defect on the wall of the CNT (first step in the unzipping process).
- Taking into account that the curvature is in the y–z direction, the PDOS analysis show increase of the DOS of $2p_z$ and $2p_y$ levels which favours the reactivity and for the ORCNT favours the spontaneous reaction.
- The unzipping process continues by the adsorption of a second permanganate group in the following parallel C–C bond, adjacent to the hole, delivering a longitudinal unzipping and yielding nanoribbons of zigzag edge. The driving force for this process is the stress generated by the repulsion between oxygen atoms in the first dione.

Acknowledgments This work was supported by PIP 11420090100066 CONICET, PICT 2010-1824, PME 2006-1581, SECyT UNC, Argentina.

References

1. Novoselov KS, Geim AK, Morozov SV, Jiang D, Zhang Y, Dubonos SV (2004) Electric field effect in atomically thin carbon films. Science 306:666–669
2. Luque GL, Rojas MI, Rivas GA, Leiva EPM (2010) The origin of the catalysis of hydrogen peroxide reduction by functionalized graphene surfaces: a density functional theory study. Electro Acta 56:523–530
3. Kuila T, Bose S, Khanra P, Mishra AK, Kim NH, Lee JH (2011) Recent advances in graphene-based biosensors. Biosens Bioelec 26(12):4637–4648
4. Gan T, Hu S (2011) Electrochemical sensors based on graphene materials. Microchim Acta 175:1–19
5. Hou J, Shao Y, Ellis MW, Moore RB, Yi B (2011) Graphene-based electrochemical energy conversion and storage: fuel cells, supercapacitors and lithium ion batteries. Phys Chem Chem Phys 13 (34):15384–15402
6. Rojas MI, Leiva EPM (2007) Density functional theory study of a graphene sheet modified with titanium in contact with different adsorbates. Phys Rev B 76(15):155415–15523
7. Sigal A, Rojas MI, Leiva EPM (2011) Interferents for hydrogen storage on graphene sheet decorated with nickel: a DFT study. Inter J Hydrog Energy 36(5):3537–3546
8. Sigal A, Rojas MI, Leiva EPM (2011) Is hydrogen storage possible in metal-doped graphite 2D systems in conditions found on earth? Phys Rev Lett 107(15):158701–158705
9. Huang X, Yin Z, Wu S, Qi X, He Q, Zhang Q, Yan Q, Boey F, Zhang H (2011) Graphene-based materials: synthesis, characterization, properties, and applications. Small 7(14):1876–1902
10. Flynn GW (2011) Perspective: the dawning of the age of graphene. J Chem Phys 135(5):050901–050909
11. Brownson DAC, Kampouris DK, Banks CE (2012) Graphene electrochemistry: fundamental concepts through to prominent applications. Chem Soc Rev 41:6944–6976
12. Sridhar V, Jeon J, Oh I (2011) Microwave extraction of graphene from carbon fibers. Carbon 49(1):222–226
13. Grayfer ED, Makotchenko VG, Nazarov AS, Kim SJ, Fedorov VE (2011) Graphene: chemical approaches to the synthesis and modification. Russ Chem Rev 80(8):751–770
14. Cho S, Kikuchi K, Kawasaki A (2011) Radial followed by longitudinal unzipping of multiwalled carbon nanotubes. Carbon 49 (12):3865–3872
15. Cataldo F, Compagnini G, Patané C, Ursini O, Angelini G, Ribic PR, Cricenti A, Palleschi G, Valentini F (2010) Graphene nanoribbons produced by the oxidative unzipping of single-wall carbon nanotubes. Carbon 48(9):2596–2602
16. Novoselov KS, Geim AK, Morozov SV, Jiang D, Katsnelson MI, Grigorieva IV, Dubonos SV, Firsov AA (2005) Two-dimensional gas of massless Dirac fermions in graphene. Nature 438:197–200
17. Castro Neto AH, Guinea F, Peres NM, Novoselov KS, Geim AK (2009) The electronic properties of graphene. Rev Modern Phys 81 (1):109–162
18. Acik M, Chabal YJ (2011) Nature of graphene edges: a review. Jap J App Phys 50:070101–070117
19. Kosynkin DV, Higginbotham AL, Sinitskii A, Lomeda JR, Dimiev A, Price BK, Tour JM (2009) Longitudinal unzipping of carbon nanotubes to form graphene nanoribbons. Nature 458:872–876
20. Higginbotham AL, Kosynkin DV, Sinitskii A, Sun Z, Tour JM (2010) Graphene oxide nanoribbons from multiwalled carbon nanotubes. ACS Nano 4(4):2059–2069
21. Ramesha GK, Sampath S (2007) Exfoliated graphite oxide modified electrode for the selective determination of picomolar concentration of lead. Electroanalytical 19(23):2472–2478
22. Bhardwaj T, Antic A, Pavan B, Barone V, Fahlman BD (2010) Enhanced electrochemical lithium storage by graphene nanoribbons. J Am Chem Soc 132:12556–12558
23. Zhang H, Zhao M, He T, Zhang X, Wang Z, Xi Z, Yan S, Xia Y, Mei L (2010) Orientation-selective unzipping of carbon nanotubes. Phys Chem Chem Phys 12(41):13674–13680

24. Rangel NL, Sotelo JC, Seminario JM (2009) Mechanism of carbon nanotubes unzipping into graphene ribbons. J Chem Phys 131 (3):31105–31109
25. Titantah JT, Jorissen K, Lamoen D (2004) Density functional theory calculations of energy-loss carbon near-edge spectra of small diameter armchair and zigzag nanotubes: core–hole, curvature, and momentum-transfer orientation effects. Phys Rev B 69:125406–125411
26. Ordejón P, Artacho E, Soler JM (1996) Self-consistent order-*N* density-functional calculations for very large systems. Phys Rev B 53(16):R10441–R10444
27. Soler JM, Artacho E, Gale JD, García A, Junquera J, Ordejón P, Sánchez-Portal D (2002) The SIESTA method for *ab initio* order-*N* materials simulation. J Phys Condens Matter 14(11):2745–2779
28. Perdew JP, Burke K, Ernzerhof M (1996) Generalized gradient approximation made simple. Phys Rev Lett 77(18):3865–3868
29. Troullier N, Martins JL (1991) Efficient pseudopotentials for plane-wave calculations. Phys Rev B 43(3):1993–2006
30. Kleinman L, Bylander DM (1982) Efficacious form for model pseudopotentials. Phys Rev Lett 48(20):1425–1428
31. Press WH, Flannery BP, Teukolsky SA, Vetterling WT (1986) Numerical recipes: the art of scientific computing. Cambridge University Press, Cambridge
32. Szabo A, Ostlund NS (1989) Modern quantum chemistry. Graw-Hill, New York
33. Robertson DH, Brenner DW, Mintmire JW (1992) Energetics of nanoscale graphitic tubules. Phys Rev B 45(21):12592–12595
34. Tibbets GG (1984) Why are carbon filaments tubular? J Cryst Growth 66(3):632–638
35. Gülseren O, Yildirim T, Ciraci S (2002) Systematic *ab initio* study of curvature effects in carbon nanotubes. Phys Rev B 65(15):153405–153409
36. Sánchez-Portal D, Artacho E, Soler J, Rubio A, Ordejón P (1999) *Ab initio* structural, elastic, and vibrational properties of carbon nanotubes. Phys Rev B 59(19):12678–12688
37. Haddon RC (1993) Chemistry of the fullerenes: the manifestation of strain in a class of continuous aromatic molecules. Science 261:1545–1550
38. Niyogi S, Hamon MA, Hu H, Zhao B, Bhowmik P, Sen R, Itkis ME, Haddon RC (2002) Chemistry of single-walled carbon nanotubes. Acc Chem Res 35:1105–1113
39. http://www.carbonsolution.com/Pyramidalization.html
40. Dinadayalane TC, Leszczynski J (2007) Towars nanomaterials: structural, energetic and reactivity aspects of single-walled carbon nanotubes. In: Balbuena P, Seminario JM (eds) Nanomaterials: design and simulation, 1st edn. Elsevier, Italy, pp 167–201
41. Haddon RC (1986) Hybridization and the orientation and alignment of.pi.-orbitals in nonplanar conjugated organic molecules:pi.-orbital axis vector analysis (POAV2). J Am Chem Soc 108(11):2837–2842
42. Haddon RC (2001) Comment on the relationship of the pyramidalization angle at a conjugated carbon atom to the σ bond angles. J Phys Chem B 105:4164–4165
43. Sun CH, Finnerty JJ, Lu GQ, Cheng HM (2005) Stability of supershort single-walled carbon nanotubes. J Phys Chem B 109:12406–12409